RESEARCH ARTICLE

Figures and figure supplements

Local angiogenic interplay of Vegfc/d and Vegfa controls brain region-specific emergence of fenestrated capillaries

Sweta Parab *et al*.

Figure 1. Genetic loss of Wnt/β-catenin signaling leads to severely impaired angiogenesis in the brain parenchyma without any apparent defect in fenestrated choroid plexus (CP) vasculature. (**A, A′**) Dorsal (**A**) and lateral (**A′**) views of a 72 hours post fertilization (hpf) *Et(cp:EGFP);Tg(kdrl:ras-mCherry)* larval head point to the locations of the diencephalic and myelencephalic CP (dCP and mCP, respectively). (**B, B′**) Dorsal (**B**) and lateral (**B′**) views of a 72 hpf *Tg(plvap:EGFP);Tg(glut1b:mCherry)* larval head indicate fenestrated and blood-brain barrier (BBB) states of meningeal and brain

Figure 1 continued on next page

Figure 1 continued

vasculature. Blood vessels formed in the dCP and mCP display strong *Tg(plvap*:EGFP) expression. (**C–C"'**) Dorsal views of the 10 days post fertilization (dpf) *Tg(plvap:EGFP);Tg(glut1b:mCherry*) larval head immunostained for P-glycoprotein (Pgp), an endothelial marker for the BBB state. Vasculature which forms in the dCP and mCP shows strong *Tg(plvap*:EGFP) expression and absent expression of both *Tg(glut1b*:mCherry) transgene and Pgp immunoreactivity. (**D–G**) Magnified, merged images of the immunostained larva shown in (**C–C"'**). In support of *Tg(plvap*:EGFP) and *Tg(glut1b*:mCherry) transgene expression, Pgp immunoreactivity was detected in *Tg(glut1b*:mCherry)$^{+}$ blood vessels, including the MsV, MCeV, and blood vessels in the midbrain parenchyma. *Tg(plvap*:EGFP)$^{+}$ blood vessels were devoid of Pgp immunoreactivity. (**H**) Schematic diagram of the dorsal view of cranial vasculature at around 72–10 dpf, illustrating the locations of the two CPs and distinct cranial blood vessels used for quantifications. **PrA**: prosencephalic artery, **PGV**: pineal gland vessel, **ACeV**: anterior cerebral vein, **MsV**: mesencephalic vein, **MCeV**: middle cerebral vein, **DLV**: dorsal longitudinal vein, **PCeV**: posterior cerebral vein. (**I–L**') Dorsal (**I–L**) and lateral (**I'–L'**) views of 72 hpf wild-type (WT) (**I, I'**), *gpr124*$^{-/-}$ (**J, J'**), *reck*$^{-/-}$ (**K, K'**), and *wnt7aa*$^{-/-}$ (**L, L'**) larval head vasculature visualized by *Tg(kdrl*:EGFP) expression. Color-coded maximum projection images indicate the most dorsal vessels in red and ventral ones in blue with a gradual color shift from dorsal to ventral (the color codes are shown in a panel left to **I'**). Asterisks indicate severely impaired angiogenesis in the brain parenchyma of these mutants compared to WT (**I'–L**'). (**M–S**) Quantification of vessel formation in the dorsal meningeal and brain compartments at 72 hpf (the number of animals examined per genotype is listed in the panel). No significant difference was detected in *gpr124*$^{-/-}$, *reck*$^{-/-}$, or *wnt7aa*$^{-/-}$ larvae compared to WT. Data are means ± SD. NS: not significant. For panels **N–S**, each data point shown in magenta represents individual animal's vessel formation score. Scale bars: 50 μm in (**A–B**'), in (**C"**') for (**C–C"'**), in (**D–G**), in (**L**) for (**I–L**), and in (**L**') for (**I'–L'**).

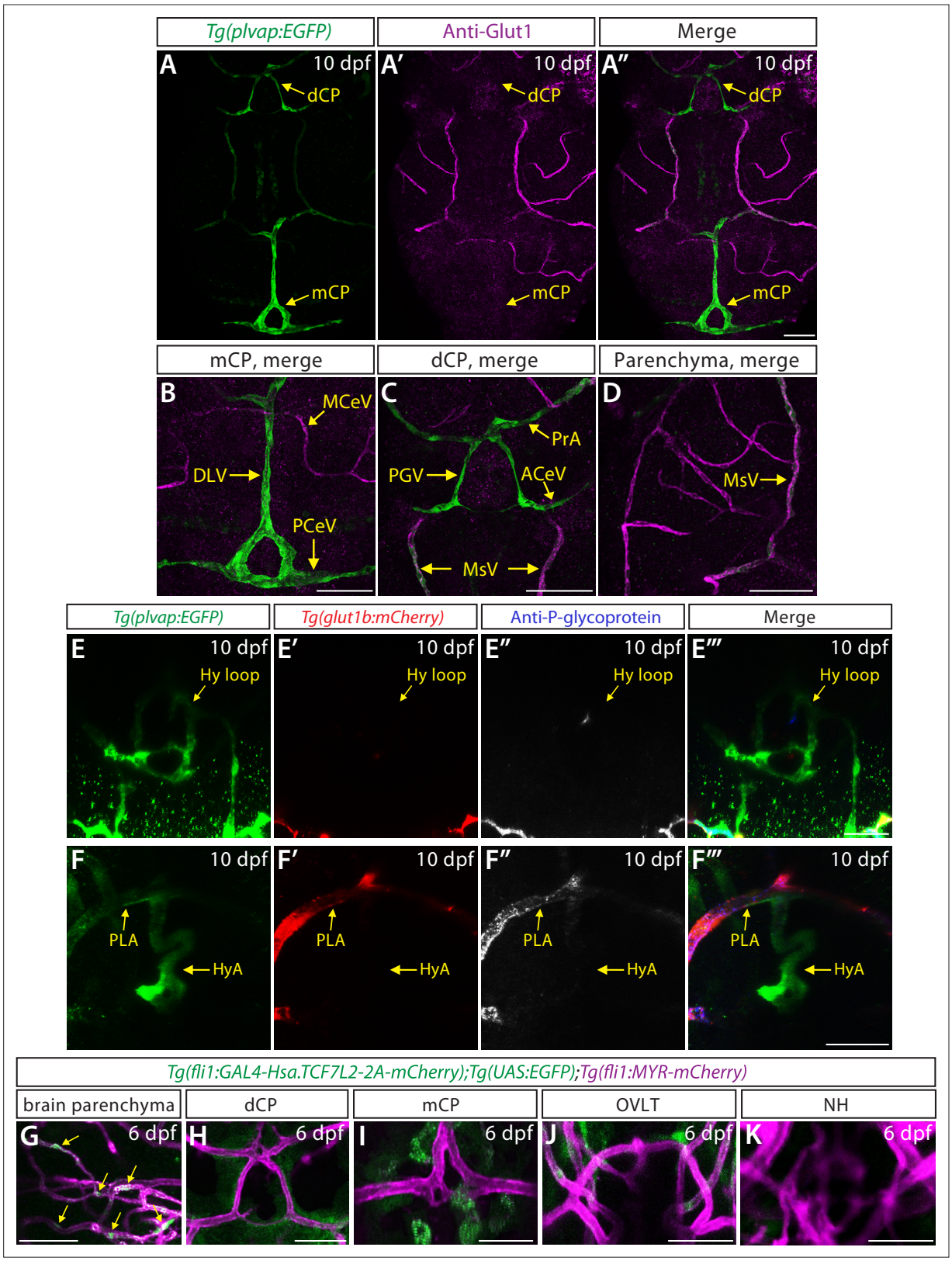

Figure 1—figure supplement 1. Characterization of endothelial marker and β-catenin reporter expression in zebrafish larval brain vasculature. (**A–A**″) Dorsal views of a 10 days post fertilization (dpf) *Tg(plvap:EGFP)* zebrafish head immunostained for Glut1, an endothelial marker for the blood-brain barrier (BBB) state. *Tg(plvap*:EGFP)$^{+}$ blood vessels formed in the diencephalic choroid plexus (dCP) and myelencephalic choroid plexus (mCP) were devoid of Glut1 immunoreactivity. (**B–D**) Magnified, merged images of the immunostained larva shown in (**A″**). Glut1 immunoreactivity

Figure 1—figure supplement 1 continued on next page

Figure 1—figure supplement 1 continued

was mostly detected in *Tg(plvap:*EGFP)$^{-}$ blood vessels in the meningeal and brain parenchymal compartments. (**E–F‴**) Dorsal views of the 10 dpf *Tg(plvap:EGFP);Tg(glut1b:mCherry*) zebrafish heads immunostained for P-glycoprotein (Pgp) shows absent expression of both the *Tg(glut1b:*mCherry) transgene and Pgp immunoreactivity in the *Tg(plvap:*EGFP)$^{+}$ Hy loop (**E–E‴**). While Pgp immunoreactivity overlapped with most *Tg(glut1b:*mCherry)$^{+}$ blood vessels (**E′, E″, F′, F″**), *Tg(plvap:*EGFP)$^{+}$ blood vessels were mostly devoid of Pgp immunoreactivity. Similar to Glut1 immunoreactivity (***Figure 2C–D″***), a rostral portion of the *Tg(plvap:*EGFP)$^{+}$ hypophyseal artery (HyA) in proximity to the organum vasculosum of the lamina terminalis (OVLT) and the palatocerebral arteries (PLA) junction was devoid of both *Tg(glut1b:*mCherry) transgene expression and Pgp immunoreactivity (**F–F‴**). (**G–K**) Magnified, merged images of 6 dpf *Tg(fli1:GAL4-Hsa.TCF7L2-2A-mCherry);Tg(UAS:EGFP);Tg(fli1:MYR-mCherry*) larvae show endothelial β-catenin reporter expression in hindbrain central arteries (**G**, arrows). This high level of endothelial β-catenin reporter expression was not detected in strong *Tg(plvap:*EGFP)$^{+}$ vasculature which forms in the dCP (**H**) and mCP (**I**) as well as in the Hy loop (**K**) and a rostral portion of the HyA (**J**). Scale bars: 50 μm in (**A″**) for (**A–A″**), in (**B–D**), and in (**G–K**); 25 μm in (**E‴**) for (**E–E‴**) and in (**F‴**) for (**F–F‴**).

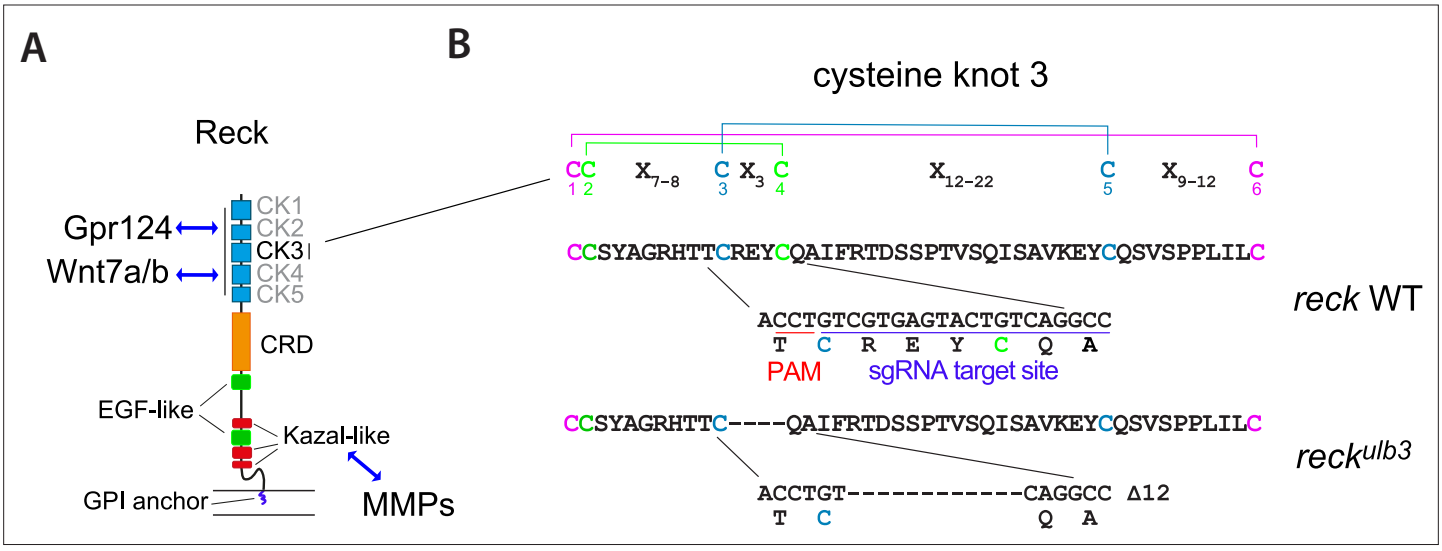

Figure 1—figure supplement 2. Characterization of the *reck*^{ulb3} allele. (**A**) Schematic representation of the domain architecture of Reck, with from N- to C-terminus, five cysteine knot (CK) motifs, a Frizzled-like cysteine-rich domain (CRD), two epidermal growth factor-like domains (EGF-like) and three Kazal-like motifs upstream of a membrane glycosylphosphatidylinositol (GPI) anchor. The CK motifs are implicated in Wnt signaling by binding Gpr124 and Wnt7a/b, while the Kazal motifs control matrix metalloproteinase (MMP) activity. (**B**) Sequence alignment of wild-type (WT) and mutant Reck sequences, showing the disulfide bonding pattern within the CK motif consensus (6 Cys repeat: C-C-X7-9-C-X3-C-X12-22-C-X9-12-C). The *reck*^{ulb3} mutant allele was generated by CRISPR-Cas9 mutagenesis at the target site highlighted in blue (see Materials and methods for details). PAM: protospacer adjacent motif. An in-frame mutation allele was selected to interfere selectively with the domains of Reck implicated in Wnt-dependent brain angiogenesis.

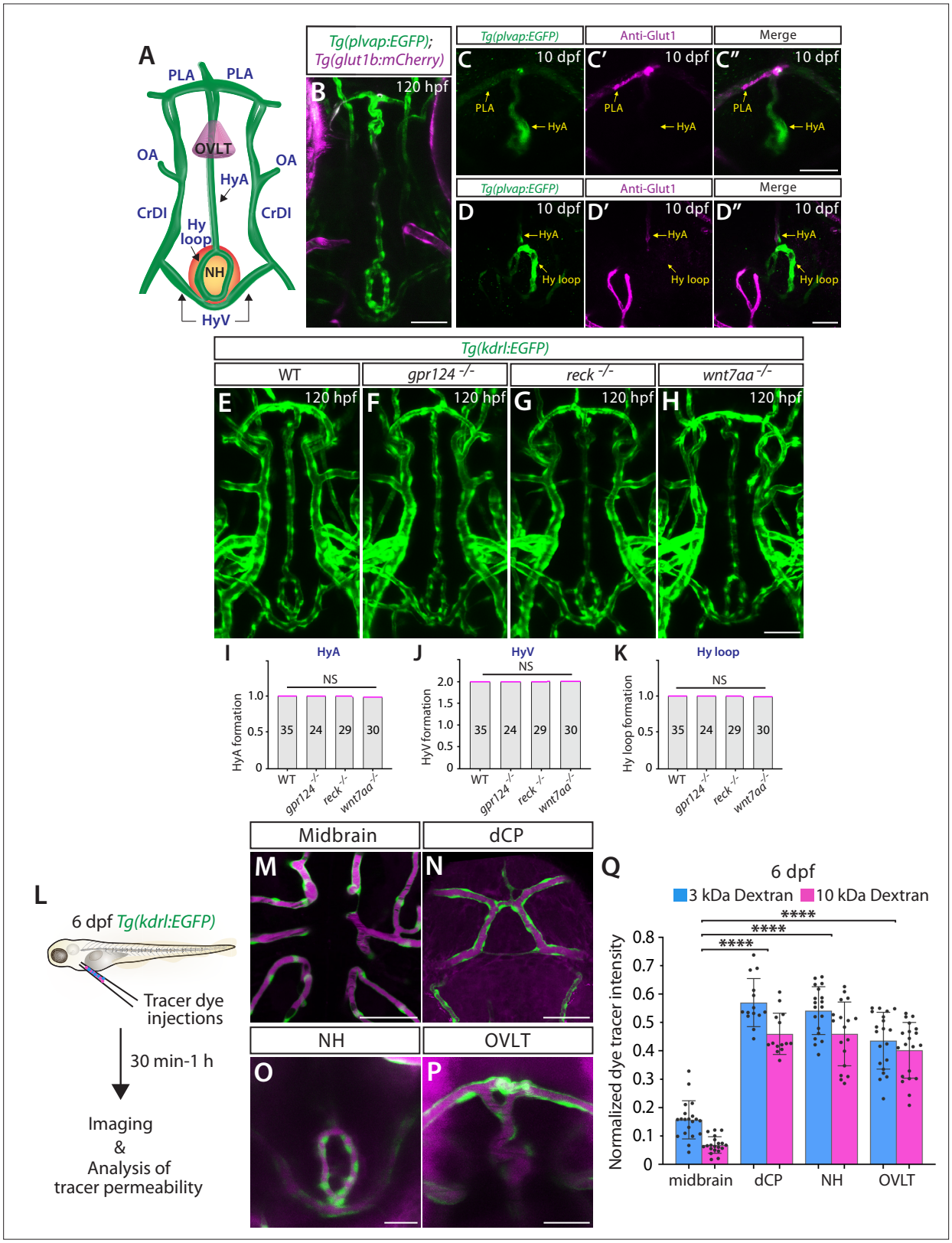

Figure 2. Wnt/β-catenin signaling deficiency does not cause any apparent defect in fenestrated capillary formation in the neurohypophysis (NH) and organum vasculosum of the lamina terminalis (OVLT). (**A**) Schematic diagram of vasculature in the ventral brain at around 5–10 days post fertilization (dpf), illustrating the locations of the OVLT, the NH, and distinct blood vessels used for quantifications. **HyA**: hypophyseal artery, **HyV**: hypophyseal veins, **Hy loop**: hypophyseal loop, **PLA**: palatocerebral arteries, **OA**: optic artery, **CrDI**: cranial division of the internal carotid artery. (**B**) Dorsal view of

Figure 2 continued on next page

Figure 2 continued

120 hours post fertilization (hpf) *Tg(plvap:EGFP);Tg(glut1b:mCherry)* ventral brain shows strong *Tg(plvap*:EGFP) expression in the Hy loop, HyA, and PLA compared to its fainter signals in the HyV. (**C–D″**) Dorsal views of the 10 dpf *Tg(plvap:EGFP)* head immunostained for Glut1. Glut1 immunoreactivity was undetectable in a rostral portion of the *Tg(plvap*:EGFP)$^{+}$ HyA that lies in proximity to the OVLT (**C–C″**) and in the *Tg(plvap*:EGFP)$^{+}$ Hy loop (**D–D″**). Faint signals were detected in a caudal portion of the HyA that resides close to the Hy loop (**D–D″**). (**E–H**) Dorsal views of 120 hpf wild-type (WT) (**E**), *gpr124*$^{-/-}$ (**F**), *reck*$^{-/-}$ (**G**), and *wnt7aa*$^{-/-}$ (**H**) ventral brain vasculature visualized by *Tg(kdrl*:EGFP) expression. *gpr124*$^{-/-}$, *reck*$^{-/-}$, or *wnt7aa*$^{-/-}$ larvae formed vasculature in the NH/OVLT regions similar to WT. (**I–K**) Quantification of ventral brain vessel formation at 120 hpf (the number of animals examined per genotype is listed in the panel). No significant difference was detected in *gpr124*$^{-/-}$, *reck*$^{-/-}$, or *wnt7aa*$^{-/-}$ larvae compared to WT. Each data point shown in magenta represents individual animal's vessel formation score. (**L**) Experimental workflow of tracer dye injections and subsequent imaging and tracer permeability analysis. *Tg(kdrl*:EGFP) larvae at 6 dpf were co-injected with 3 kDa and 10 kDa dextran dyes conjugated with different fluorophores. (**M–P**) Merged images of 3 kDa tetramethylrhodamine-conjugated dextran dye (magenta) and *Tg(kdrl*:EGFP)$^{+}$ vasculature at 6 dpf. Unlike the midbrain parenchyma (**M**) where a functional blood-brain barrier (BBB) is established, a higher amount of tracer accumulation was detected in tissues around the diencephalic choroid plexus (dCP), NH, and OVLT brain regions (**N–P**). (**Q**) Quantification of normalized tracer intensity across the different brain regions at 6 dpf reveals a significant increase in tracer accumulation around the dCP, NH, and OVLT brain regions compared to the midbrain parenchyma. **** indicates $p<0.0001$ by one-way analysis of variance (ANOVA) followed by Tukey's HSD test. Statistical significance was calculated for each dye tracer across different brain regions and represents differences in the graph. Scale bars: 50 μm in (**B**), in (**H**) for (**E–H**), in (**M–N**); 25 μm in (**C″**) for (**C–C″**), in (**D″**) for (**D–D″**), in (**O–P**).

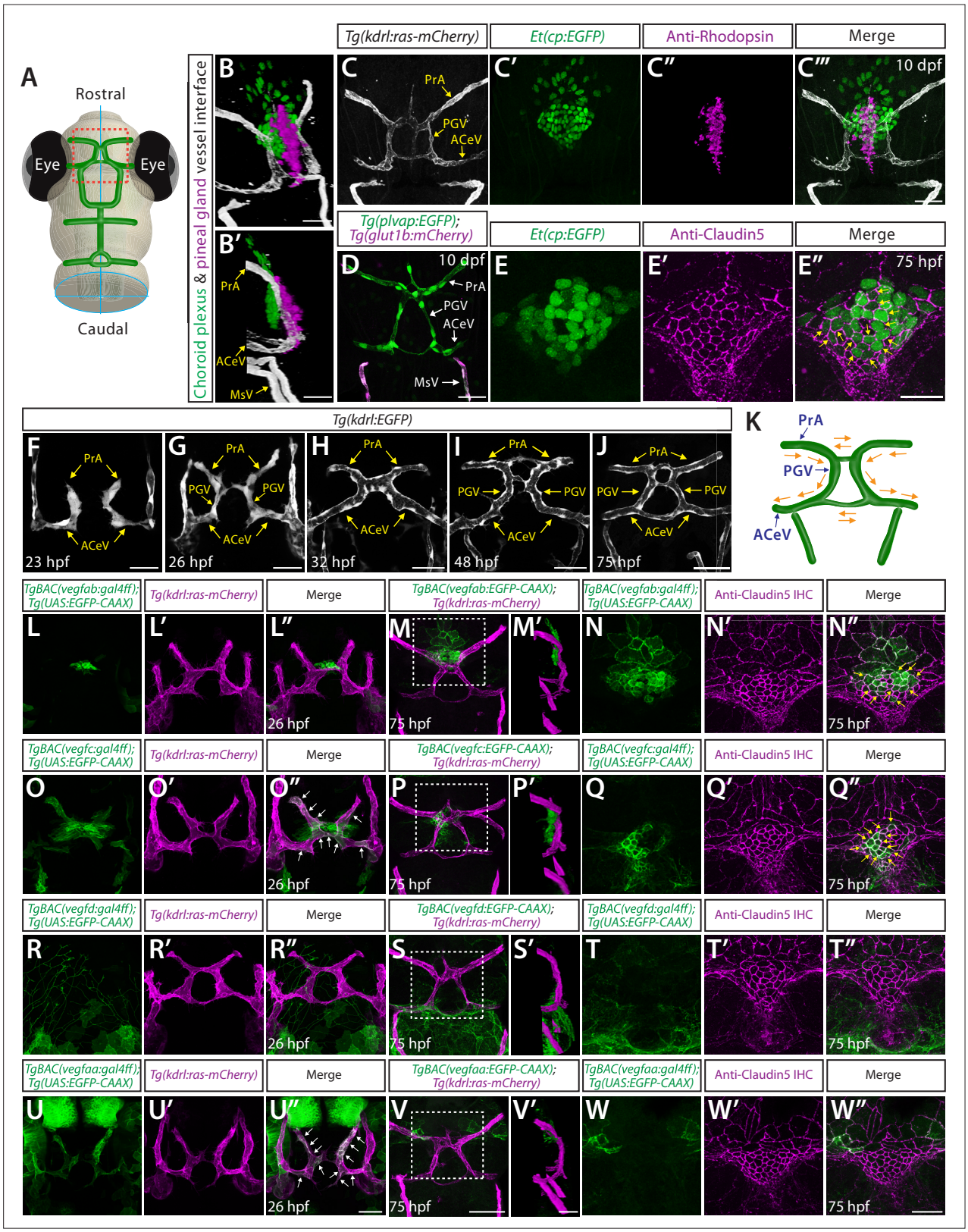

Figure 3. Developmental angiogenesis at the interface of the diencephalic choroid plexus (dCP) and pineal gland (PG), and *vegf* expression patterns during the vascularization of this interface. (**A**) Schematic representation of the dorsal view of the zebrafish larval head at 10 days post fertilization (dpf), indicating the location of the dCP and PG interface (red boxed area). (**B–C‴**) 3D (**B**), lateral (**B′**), and dorsal (**C–C‴**) views of the 10 dpf *Et(cp:EGFP);Tg(kdrl:ras-mCherry)* head immunostained for rhodopsin show the 3D spatial relationship between dCP epithelial cells (green),

Figure 3 continued on next page

Figure 3 continued

pineal photoreceptor cells (magenta), and blood vessels (white). (**D**) Dorsal view of 10 dpf *Tg(plvap:EGFP);Tg(glut1b:mCherry)* head shows strong *Tg(plvap:*EGFP) and undetectable *Tg(glut1b:*mCherry) expression in the prosencephalic artery (PrA), PG vessel (PGV), and anterior cerebral vein (ACeV). In contrast, the neighboring vessels mesencephalic vein (MsV) display strong *Tg(glut1b:*mCherry) expression. (**E–E″**) Dorsal views of the 75 hours post fertilization (hpf) *Et(cp:EGFP)* head immunostained for Claudin-5 show EGFP$^+$ dCP epithelial cells (yellow arrows) outlined by the tight junction protein Claudin-5. (**F–J**) Dorsal views of 23 (**F**), 26 (**G**), 32 (**H**), 48 (**I**), and 75 (**J**) hpf *Tg(kdrl:EGFP)* rostral cranial vasculature show the developmental time courses of vascularization at the dCP/PG interface. (**K**) Schematic diagram of the vasculature at the dCP/PG interface shows the direction of blood flow at around 75–10 dpf. (**L–L″**) Dorsal views of a 26 hpf *TgBAC(vegfab:EGFP);Tg(kdrl:ras-mCherry)* head show *TgBAC(vegfab:*EGFP)$^+$ cells at the midline where bilateral PrA connect. (**M–N″**) Dorsal (**M–N″**) and lateral (**M′**) views of a 75 hpf *TgBAC(vegfab:EGFP);Tg(kdrl:ras-mCherry)* head immunostained for Claudin-5. As compared to 26 hpf, an increased number of *TgBACvegfab:*EGFP $^+$ cells was observed at the PrA connection site and in its anterior brain regions (**M, M′**). Magnified images of the boxed area in (**M**) indicate *TgBAC(vegfab:*EGFP)$^+$ and Claudin-5$^+$ dCP epithelial cells (yellow arrows, **N–N″**). (**O–O″**) Dorsal views of a 26 hpf *TgBAC(vegfc:EGFP);Tg(kdrl:ras-mCherry)* head show *TgBAC(vegfc:*EGFP)$^+$ vascular endothelial cells (vECs, white arrows) and separate cells at the PrA connection site. (**P–Q″**) Dorsal (**P**, **Q–Q″**) and lateral (**P′**) views of a 75 hpf *TgBAC(vegfc:EGFP);Tg(kdrl:ras-mCherry)* head immunostained for Claudin-5. *TgBAC(vegfc:*EGFP)$^+$ cells were observed at the PrA connection site and in its posterior brain regions (**P, P′**). Magnified images of the boxed area in (**P**) indicate *TgBAC(vegfc:*EGFP)$^+$ and Claudin-5$^+$ dCP epithelial cells (yellow arrows, **Q–Q″**). (**R–R″**) Dorsal views of a 26 hpf *TgBAC(vegfd:EGFP);Tg(kdrl:ras-mCherry)* head show *TgBAC(vegfd:*EGFP)$^+$ meningeal fibroblast-like cells that reside posterior to the dCP/PG interface. *TgBAC(vegfd:*EGFP)$^+$ axonal projections were also visualized. (**S–T″**) Dorsal (**S, T–T″**) and lateral (**S′**) views of a 75 hpf *TgBAC(vegfd:EGFP);Tg(kdrl:ras-mCherry)* head immunostained for Claudin-5. *TgBAC(vegfd:*EGFP)$^+$ cells were observed in meningeal fibroblast-like cells that reside posterior to the PGV/ACeV (**S, S′**). Magnified images of the boxed area in (**S**) show no obvious *TgBAC(vegfd:*EGFP) expression in dCP epithelial cells (**T–T″**). (**U–U″**) Dorsal views of a 26 hpf *TgBAC(vegfaa:EGFP);Tg(kdrl:ras-mCherry)* head show *TgBAC(vegfaa:*EGFP)$^+$ vECs (white arrows). (**V–W″**) Dorsal (**V**, **W–W″**) and lateral (**V′**) views of a 75 hpf *TgBAC(vegfaa:EGFP);Tg(kdrl:ras-mCherry)* head immunostained for Claudin-5. Sparse *TgBAC(vegfaa:*EGFP)$^+$ cells were observed at the lateral periphery of the dCP (**W-W′**). Magnified images of the boxed area in (**V**) show *TgBAC(vegfaa:*EGFP)$^+$ and Claudin-5$^+$ dCP epithelial cells at the periphery (**W-W′**). Scale bars: 30 μm in (**B**), (**B′**), (**D**), in (**C″′**) for (**C–C″′**), in (**E″**) for (**E–E″**), in (**V′**) for (**M′**), (**P′**), (**S′**); 50 μm in (**F–J**), in (**U″**) for (**L–L″**), (**O–O″**), (**R–R″**), (**U–U″**), in (**V**) for (**M**), (**P**), (**S**), in (**W″**) for (**N–N″**), (**Q–Q″**), (**T–T″**), (**W–W″**).

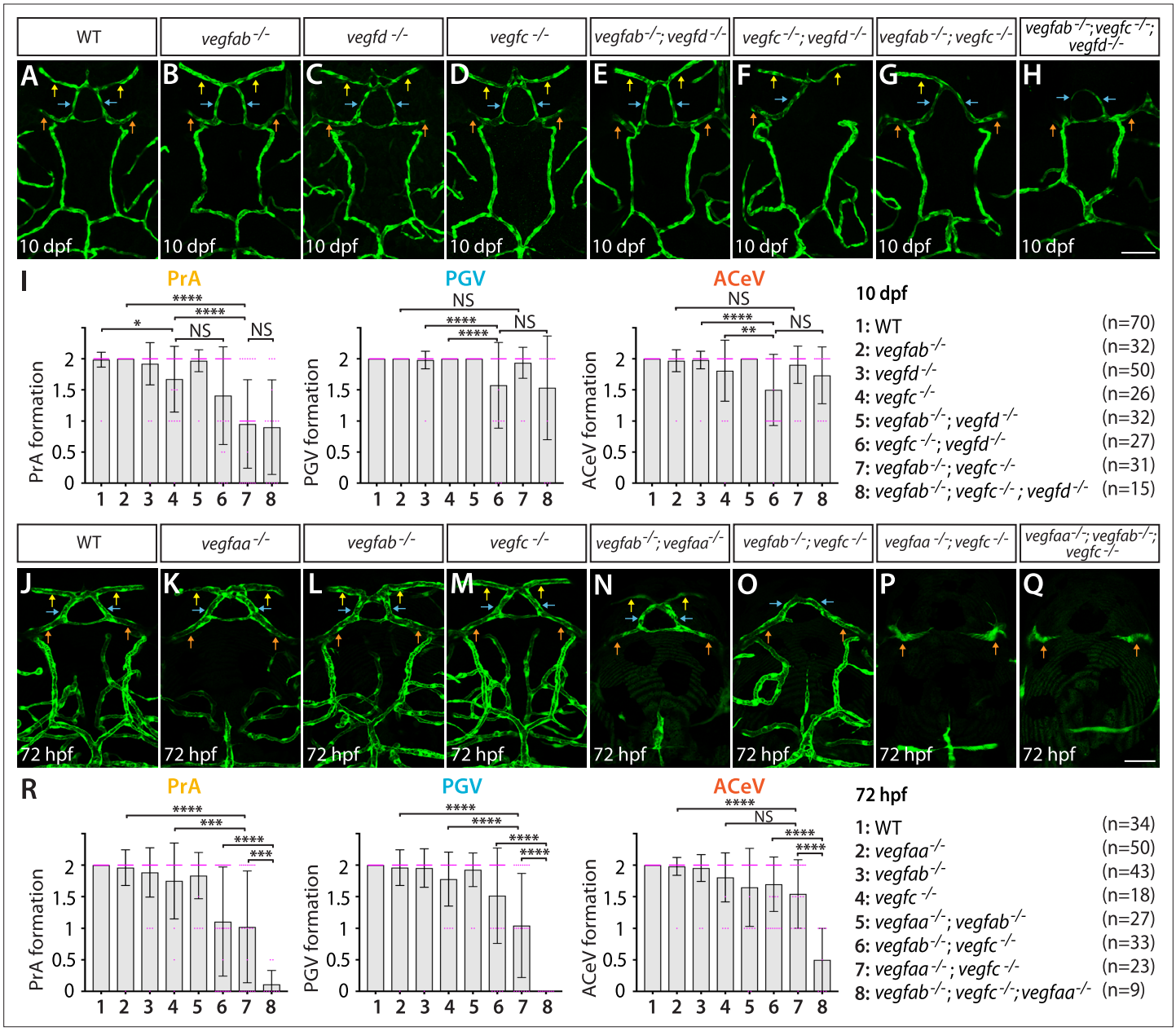

Figure 4. Heterogeneous endothelial requirements for Vegfs-dependent angiogenesis at the diencephalic choroid plexus (dCP)/pineal gland (PG) interface. (**A–H**) Dorsal views of 10 days post fertilization (dpf) wild-type (WT) (**A**), *vegfab*$^{-/-}$ (**B**), *vegfd*$^{-/-}$ (**C**), *vegfc*$^{-/-}$ (**D**), *vegfab*$^{-/-}$;*vegfd*$^{-/-}$ (**E**), *vegfc*$^{-/-}$;*vegfd*$^{-/-}$ (**F**), *vegfab*$^{-/-}$;*vegfc*$^{-/-}$ (**G**), and *vegfab*$^{-/-}$;*vegfc*$^{-/-}$;*vegfd*$^{-/-}$ (**H**) cranial vasculature visualized by *Tg(kdrl*:EGFP) expression. Yellow arrows point to the prosencephalic artery (PrA), blue arrows to the PG vessel (PGV), and orange arrows to the anterior cerebral vein (ACeV). A majority of *vegfab*$^{-/-}$;*vegfc*$^{-/-}$ (**G**) and *vegfab*$^{-/-}$;*vegfc*$^{-/-}$;*vegfd*$^{-/-}$ (**H**) larvae lacked the PrA at either or both sides. *vegfc*$^{-/-}$;*vegfd*$^{-/-}$ (**F**) and *vegfab*$^{-/-}$;*vegfc*$^{-/-}$;*vegfd*$^{-/-}$ (**H**), but not *vegfab*$^{-/-}$;*vegfc*$^{-/-}$ (**G**), larvae displayed partially penetrant defects in PGV and/or ACeV formation. (**I**) Quantification of PrA, PGV, and ACeV formation at 10 dpf (the number of animals examined per genotype is listed in the panel). Statistical data support genetic interactions between *vegfab* and *vegfc* in PrA formation and between *vegfd* and *vegfc* in PGV and ACeV formation. No significant contributions of *vegfd* or *vegfab* to the formation of the PrA or PGV/ACeV, respectively, were noted. (**J–Q**) Dorsal views of 72 hours post fertilization (hpf) WT (**J**), *vegfaa*$^{-/-}$ (**K**), *vegfab*$^{-/-}$ (**L**), *vegfc*$^{-/-}$ (**M**), *vegfab*$^{-/-}$;*vegfaa*$^{-/-}$ (**N**), *vegfab*$^{-/-}$;*vegfc*$^{-/-}$ (**O**), *vegfaa*$^{-/-}$;*vegfc*$^{-/-}$ (**P**), and *vegfaa*$^{-/-}$;*vegfab*$^{-/-}$;*vegfc*$^{-/-}$ (**Q**) cranial vasculature visualized by *Tg(kdrl*:EGFP) expression. Yellow arrows point to the PrA, blue arrows to the PGV, and orange arrows to the ACeV. *vegfab*$^{-/-}$;*vegfc*$^{-/-}$, but not their respective single mutants, exhibited pronounced PrA formation deficits. *vegfaa*$^{-/-}$ and *vegfab*$^{-/-}$;*vegfaa*$^{-/-}$ displayed severe defects in mesencephalic vein (MsV) formation without a deficit in PrA, PGV, or ACeV development. *vegfaa*$^{-/-}$;*vegfc*$^{-/-}$ and *vegfaa*$^{-/-}$;*vegfab*$^{-/-}$;*vegfc*$^{-/-}$ larvae exhibited a severe loss of the PrA and PGV. (**R**) Quantification of PrA, PGV, and ACeV formation at 72 hpf (the number of animals examined per genotype is listed in the panel). Statistical data support genetic interactions between *vegfab* and *vegfc* in PrA formation and between *vegfaa* and *vegfc* in PrA and PGV formation. Furthermore, significant genetic interactions among these three genes were detected in vascularization at this interface. In panels (**I and R**), each data point shown in magenta

Figure 4 continued on next page

Figure 4 continued

represents individual animal's vessel formation score, and values represent means ± SD (*, **, ***, and **** indicate $p<0.05$, $p<0.01$, $p<0.001$, and $p<0.0001$, respectively, by one-way analysis of variance [ANOVA] followed by Tukey's HSD test). Scale bars: 50 μm in (**H**) for (**A–H**) and in (**Q**) for (**J–Q**).

Figure 5. Endothelial cell-autonomous and cell non-autonomous requirements of Vegfc for vascularization of the diencephalic choroid plexus (dCP)/pineal gland (PG) interface. (**A–E**) Dorsal views of 72 hours post fertilization (hpf) wild-type (WT) (**A**), *vegfc*$^{um18/um18}$ (**B**), *vegfab*$^{-/-}$ (**C**), and *vegfab*$^{-/-}$;*vegfc*$^{um18/um18}$ (**D, E**) cranial vasculature visualized by *Tg(kdrl:*EGFP) expression. Yellow arrows point to the prosencephalic artery (PrA), blue arrows to the PG vessel (PGV), and orange arrows to the anterior cerebral vein (ACeV). Although none of *vegfc*$^{um18/um18}$ and *vegfab*$^{-/-}$ fish exhibited a defect in PrA

Figure 5 continued on next page

Figure 5 continued

formation (**B, C**), approximately 21% of *vegfab*$^{-/-}$;*vegfc*$^{um18/um18}$ larvae lacked the PrA at either or both sides (**E**). (**F**) Quantification of PrA, PGV, and ACeV formation at 72 hpf (the number of animals examined per genotype is listed in the panel). Specific defect was observed in PrA formation in *vegfab*$^{-/-}$;*vegfc*$^{um18/um18}$ larvae compared to other three genotypes. (**G, H**) Dorsal views of 72 hpf *vegfaa*$^{-/-}$ (**G**) and *vegfaa*$^{-/-}$;*vegfc*$^{um18/um18}$ (**H**) cranial vasculature visualized by *Tg(kdrl:*EGFP) expression. Yellow arrows point to the PrA, blue arrows to the PGV, and orange arrows to the ACeV. Although *vegfaa*$^{-/-}$ or *vegfc*$^{um18/um18}$ larvae fully formed vasculature at the dCP/PG interface, most of *vegfaa*$^{-/-}$;*vegfc*$^{um18/um18}$ larvae failed to form the PrA and PGV at either or both sides. (**I**) Quantification of PrA formation at 72 hpf (the number of animals examined per genotype is listed in the panel). The quantitative results of several genotypes were presented again or integrated in this graph for comparison purposes. Previously presented results are the *vegfc*$^{-/-}$ (*hu6410* allele) data from ***Figure 4R***, and the data in (**F**) were either re-presented or combined with the quantitative results shown in ***Figure 5G and H***. Paracrine activity-deficient *vegfc*$^{um18/um18}$ larvae in the *vegfab*$^{-/-}$ background displayed a significantly milder defect in PrA formation than that observed in *vegfab*$^{-/-}$;*vegfc*$^{-/-}$ (*hu6410* allele) animals that lack both endothelial cell-autonomous and cell non-autonomous Vegfc function. (**J**) Quantification of mesencephalic vein (MsV) formation at 72 hpf (the number of animals examined per genotype is listed in the panel). Severe defects in MsV formation in *vegfaa*$^{-/-}$ larvae were further exacerbated by genetic deletions of *vegfc* (*um18* allele) or *vegfab*. (**K**) Schematic representations of the severe vascular phenotypes observed in 72 hpf various *vegf* mutants at the dCP/PG interface. Genetic results indicate highly heterogeneous molecular requirements for angiogenesis around the dCP/PG interface. In panels (**F**), (**I**), and (**J**), each data point shown in magenta represents individual animal's vessel formation score, and values represent means ± SD (*, **, and **** indicate $p<0.05$, $p<0.01$, and $p<0.0001$, respectively, by one-way analysis of variance [ANOVA] followed by Tukey's HSD test). Scale bars: 50 μm in (**A**) for (**A–E**) and in (**G**) for (**G–H**).

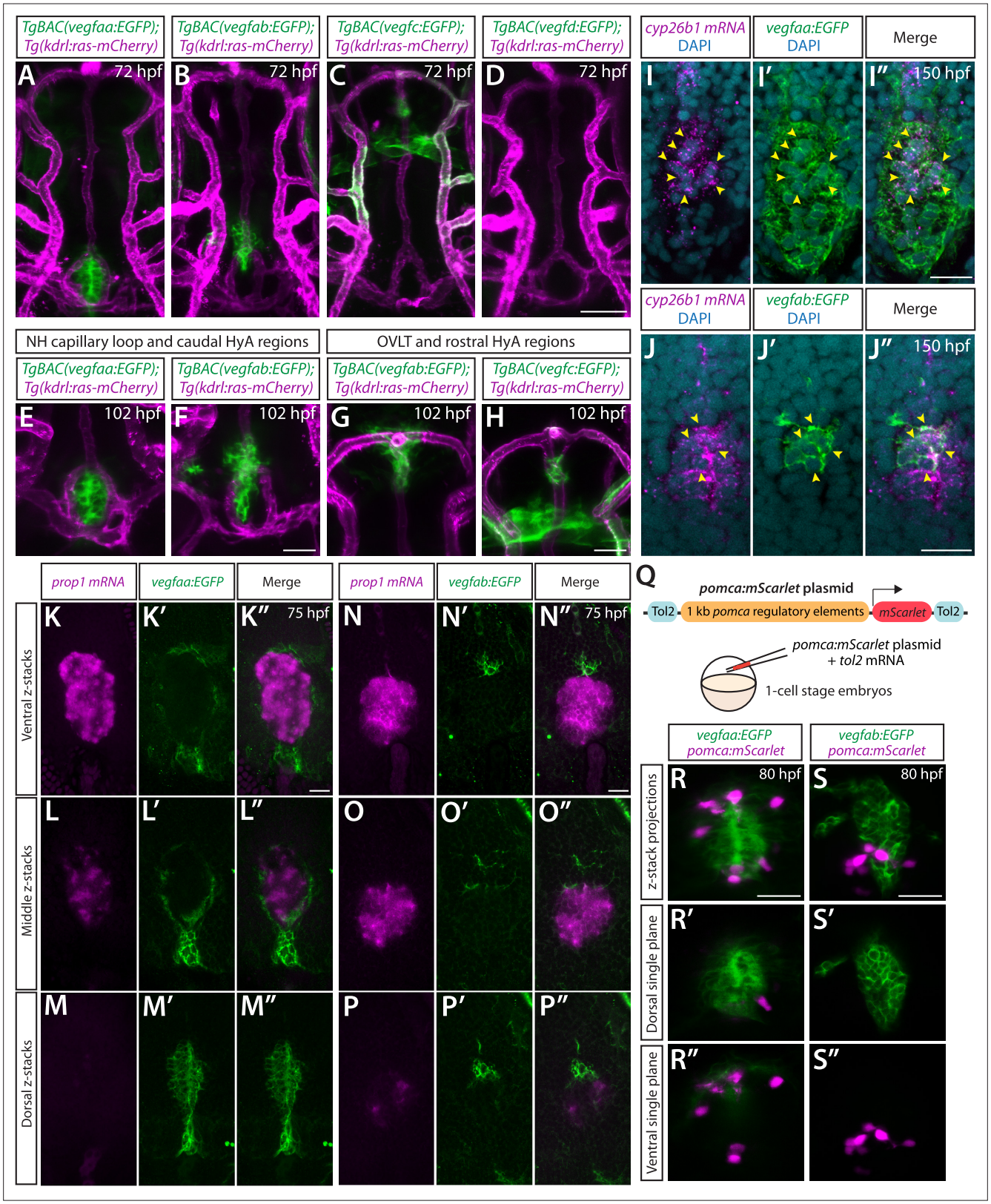

Figure 6. BAC transgenic analysis of *vegf* expression in the ventral brain around the neurohypophysis (NH)/organum vasculosum of the lamina terminalis (OVLT). (**A–D**) Dorsal views of 72 hours post fertilization (hpf) *TgBAC(vegfaa:EGFP)* (**A**), *TgBAC(vegfab:EGFP)* (**B**), *TgBAC(vegfc:EGFP)* (**C**), and *TgBAC(vegfd:EGFP)* (**D**) ventral brain of the larvae carrying the *Tg(kdrl:ras-mCherry)* transgene. Prominent *TgBAC(vegfaa*:EGFP) and *TgBAC(vegfab*:EGFP) expression was observed in cells that reside in close proximity to Hy loop at the NH (**A, B**). Notable *TgBAC(vegfc*:EGFP)

Figure 6 continued on next page

Figure 6 continued

expression was detected in the rostral portion of the hypophyseal artery (HyA) around the OVLT (**C**). *TgBAC(vegfd:*EGFP) expression was not detectable at this stage (**D**). (**E–H**) Magnified images of 102 hpf *TgBAC(vegfaa:EGFP*) (**E**), *TgBAC(vegfab:EGFP*) (**F, G**), and *TgBAC(vegfc:EGFP*) (**H**) ventral brain of the larvae carrying the *Tg(kdrl:ras-mCherry*) transgene. While *TgBAC(vegfaa:*EGFP)$^+$ cells reside slightly dorsal to the Hy loop (**E**), many *TgBAC(vegfab:*EGFP)$^+$ cells were located further rostrodorsally likely in the hypothalamus (**F**). In the rostral part of the HyA around the HyA-palatocerebral arteries (PLA) junction and OVLT, *TgBAC(vegfab:*EGFP) and *TgBAC(vegfc:*EGFP) expression was detected in peri-vascular cells (**G, H**). Additionally, strong *TgBAC(vegfc:*EGFP) signals were observed around the OVLT. (**I–I″**) Single confocal z-plane images of 150 hpf *TgBAC(vegfaa:EGFP*) ventral brain following in situ hybridization of *cyp26b1*, showing overlapping signals (yellow arrowheads) between the EGFP$^+$ cells and *cyp26b1*$^+$ pituicyte (n=10). (**J–J″**) Single confocal z-plane images of 150 hpf *TgBAC(vegfab:EGFP*) larval ventral brain following in situ hybridization of *cyp26b1*, showing overlapping signals (yellow arrowheads) between the EGFP$^+$ cells and *cyp26b1*$^+$ pituicyte (n=11). (**K–M″**) Serial confocal z-stacks of ventral (**K–K″**), middle (**L–L″**), and dorsal (**M–M″**) images showing no overlapping signals between *TgBAC(vegfaa:*EGFP)$^+$ and *prop1*$^+$ by in situ hybridization in 75 hpf larvae (n=8). (**N–P″**) Serial confocal z-stacks of ventral (**N–N″**), middle (**O–O″**), and dorsal (**P–P″**) images showing no overlapping signals between *TgBAC(vegfab:*EGFP)$^+$ and *prop1*$^+$ by in situ hybridization in 75 hpf larvae (n=10). (**Q**) Schematic of the *pomca:mScarlet* construct used for injection experiments (**R–S″**). (**R–S″**) Magnified dorsal views of 80 hpf *TgBAC(vegfaa:EGFP*) (**R–R″**) and *TgBAC(vegfab:EGFP*) (**S–S″**) NH of larvae injected with the *pomca:mScarlet* construct at the one-cell stage. Confocal z-stack maximum projection (**R, S**) and their dorsal (**R′, S′**) and ventral (**R″, S″**) single z-plane images showed no overlapping signals between EGFP$^+$ cells and *pomca:*mScarlet$^+$ pituitary corticotrophs. Scale bars: 50 μm in (**D**) for (**A–D**); 25 μm in (**F**) for (**E–F**), in (**H**) for (**G–H**), in (**R**) for (**R–R″**), in (**S**) for (**S–S″**); and 15 μm in (**I″**) for (**I–I″**), in (**J″**) for (**J–J″**), in (**K″**) for (**K–M″**), in (**N″**) for (**N–P″**).

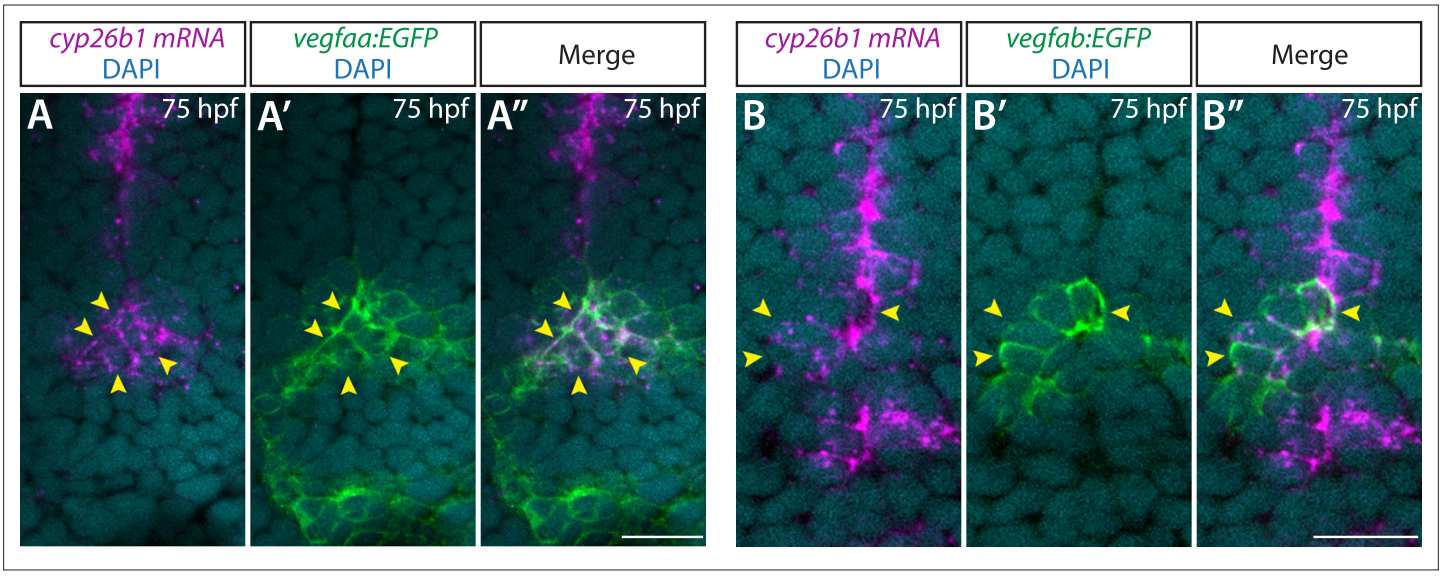

Figure 6—figure supplement 1. Co-localization of the pituicyte marker *cyp26b1* and *vegfaa* or *vegfab* BAC transgenic reporter expression at early larval stages. (**A–A″**) Single confocal *z*-plane images of 75 hours post fertilization (hpf) *TgBAC(vegfaa:EGFP)* ventral brain following in situ hybridization of *cyp26b1*, showing overlapping signals between the EGFP$^+$ cells and *cyp26b1*$^+$ pituicyte (n=10). Yellow arrowheads indicate the overlapping cells. (**B–B″**) Single confocal *z*-plane images of 75 hpf *TgBAC(vegfab:EGFP)* ventral brain following in situ hybridization of *cyp26b1*, showing overlapping signals between the EGFP$^+$ cells and *cyp26b1*$^+$ pituicyte (n=11). Yellow arrowheads indicate the overlapping cells.

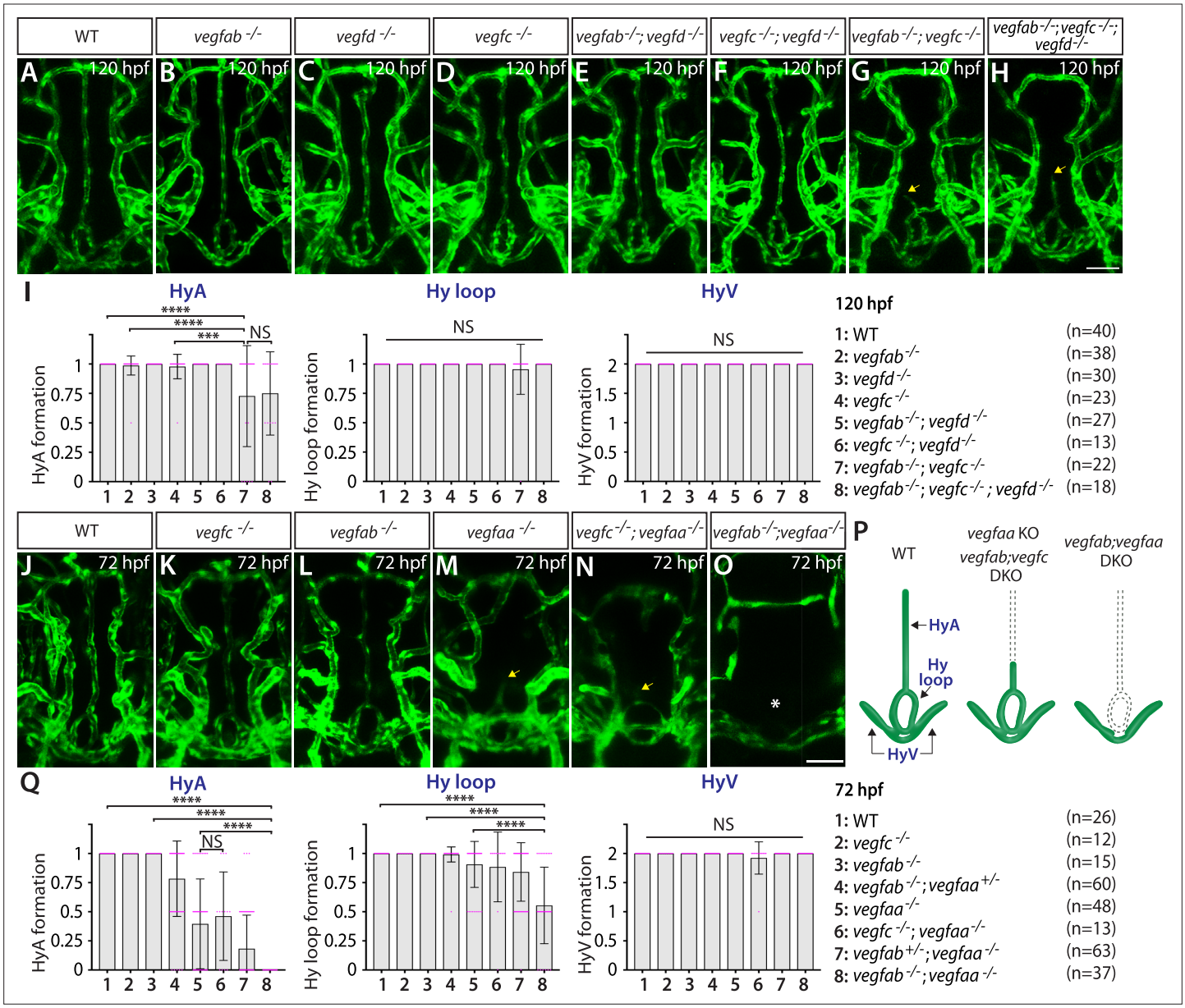

Figure 7. Heterogeneous endothelial requirements for Vegfs-dependent angiogenesis in the ventral brain around the neurohypophysis (NH)/organum vasculosum of the lamina terminalis (OVLT). (**A–H**) Dorsal views of 120 hours post fertilization (hpf) wild-type (WT) (**A**), *vegfab*$^{-/-}$ (**B**), *vegfd*$^{-/-}$ (**C**), *vegfc*$^{-/-}$ (**D**), *vegfab*$^{-/-}$;*vegfd*$^{-/-}$ (**E**), *vegfc*$^{-/-}$;*vegfd*$^{+/-}$ (**F**), *vegfab*$^{-/-}$;*vegfc*$^{-/-}$ (**G**), and *vegfab*$^{-/-}$;*vegfc*$^{-/-}$;*vegfd*$^{-/-}$ (**H**) ventral brain vasculature visualized by *Tg(kdrl*:EGFP) expression. A significant fraction of *vegfab*$^{-/-}$;*vegfc*$^{-/-}$ (**G**) and *vegfab*$^{-/-}$;*vegfc*$^{-/-}$;*vegfd*$^{+/-}$ (**H**) larvae exhibited a partial formation of the hypophyseal artery (HyA), resulting in HyA stalling toward the palatocerebral arteries (PLA) (arrows, **G, H**). (**I**) Quantification of HyA, Hy loop, and hypophyseal vein (HyV) formation at 120 hpf (the number of animals examined per genotype is listed in the panel). *vegfab*$^{-/-}$;*vegfc*$^{-/-}$ and *vegfab*$^{-/-}$;*vegfc*$^{-/-}$;*vegfd*$^{+/-}$ larvae displayed a specific and partially penetrant defect in HyA formation. (**J–O**) Dorsal views of 72 hpf WT (**J**), *vegfc*$^{-/-}$ (**K**), *vegfab*$^{-/-}$ (**L**), *vegfaa*$^{-/-}$ (**M**), *vegfc*$^{-/-}$;*vegfaa*$^{-/-}$ (**N**), and *vegfab*$^{-/-}$;*vegfaa*$^{-/-}$ (**O**) ventral brain vasculature visualized by *Tg(kdrl*:EGFP) expression. Similar to *vegfab*$^{-/-}$;*vegfc*$^{-/-}$ larvae, *vegfaa*$^{-/-}$ fish exhibited a specific and partially penetrant defect in HyA formation, leading to HyA stalling toward the PLA (arrow, **M**). The severity of this phenotype was exacerbated by the simultaneous deletion of *vegfab* (**O**), but not of *vegfc* (arrow, **N**), showing a genetic interaction between *vegfaa* and *vegfab*, but not between *vegfaa* and *vegfc*. Intriguingly, phenotypes in *vegfab*$^{-/-}$;*vegfaa*$^{-/-}$ larvae were restricted to the fenestrated HyA and Hy loop (asterisk, **O**) with no significant defect in HyV formation. (**P**) Schematic representations of the severe vascular phenotypes observed in 72 hpf various *vegf* mutants. (**Q**) Quantification of HyA, Hy loop, and HyV formation at 72 hpf. In panels (**I and Q**), each data point shown in magenta represents individual animal's vessel formation score, and values represent means ± SD (*** and **** indicate $p<0.001$ and $p<0.0001$, respectively, by one-way analysis of variance [ANOVA] followed by Tukey's HSD test). Scale bars: 50 μm in (**H**) for (**A–H**) and in (**O**) for (**J–O**).

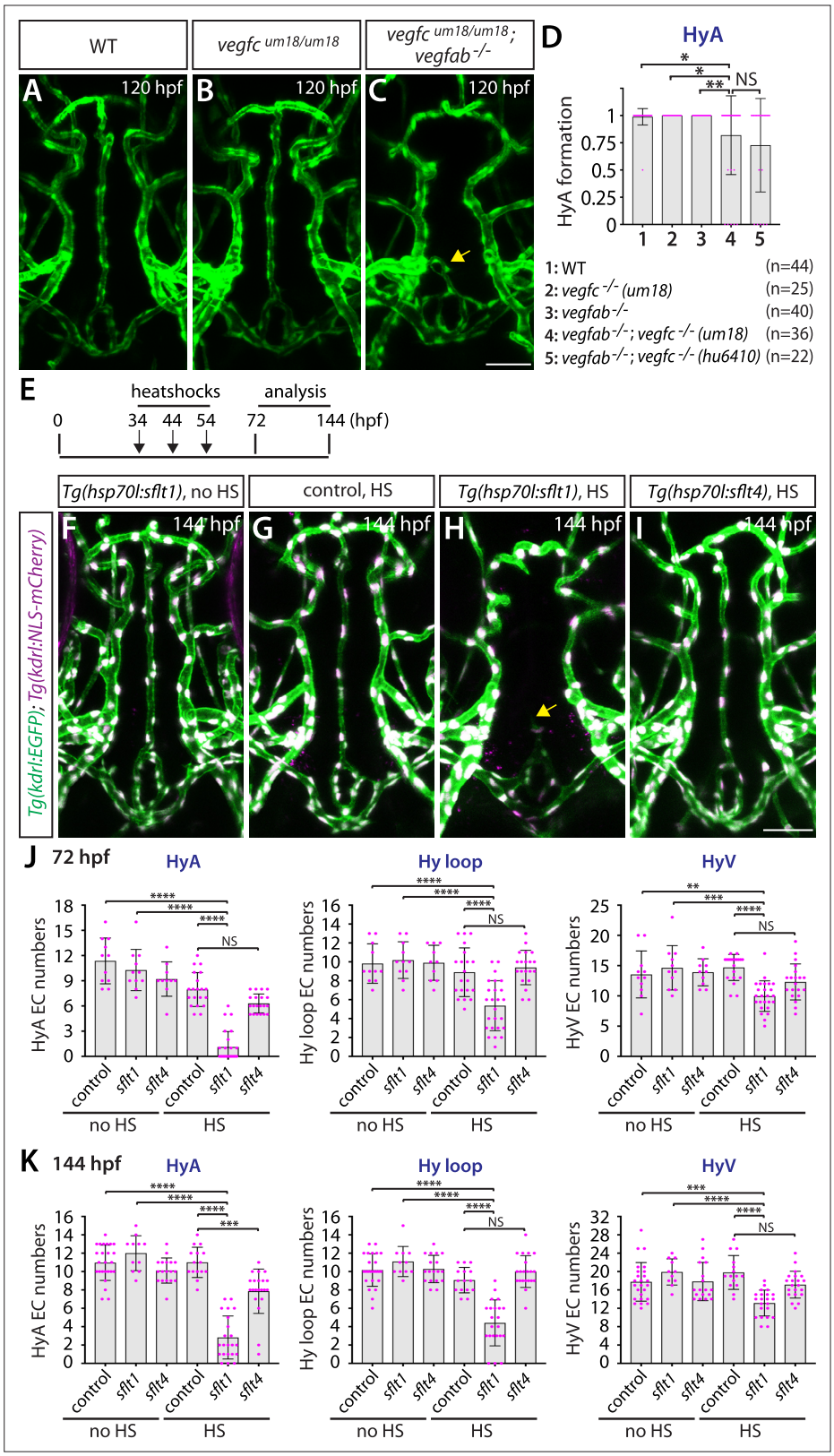

Figure 8. Temporal inhibition of Vegfa signaling by sFlt1 overexpression is sufficient to cause impaired formation of the hypophyseal artery (HyA) and Hy loop. (**A–C**) Dorsal views of 72 hours post fertilization (hpf) wild-type (WT) (**A**), *vegfc*$^{um18/um18}$ (**B**), and *vegfc*$^{um18/um18}$;*vegfab*$^{-/-}$ (**C**) ventral brain vasculature visualized by *Tg(kdrl*:EGFP) expression. *vegfc*$^{um18/um18}$;*vegfab*$^{-/-}$ larvae exhibited partial formation of the HyA, resulting in HyA stalling toward

Figure 8 continued on next page

Figure 8 continued

the palatocerebral arteries (PLA) (arrow, **C**). (**D**) Quantification of HyA formation at 120 hpf (the number of animals examined per genotype is listed in the panel). *vegfc*$^{um18/um18}$;*vegfab*$^{-/-}$ larvae exhibited a significantly increased defect in HyA formation at a comparable level to that observed in *vegfab*$^{-/-}$;*vegfc*$^{-/-}$ (*hu6410* allele) animals. The HyA quantitative results of *vegfab*$^{-/-}$;*vegfc*$^{-/-}$ (*hu6410* allele) larvae from ***Figure 7I*** were integrated in this graph for comparison purposes. (**E**) Time course of the heatshock (HS) experiments for panels (**F–I**). (**F–I**) Dorsal views of ventral brain vasculature in 144 hpf *Tg(hsp70l:sflt1)* (**F, H**), *Tg(hsp70l:sflt4)* (**I**), and their control sibling (**G**) larvae that carried both the *Tg(kdrl:EGFP)* and *Tg(kdrl:NLS-mCherry)* transgenes after treatment with (**G–I**) and without (**F**) multiple HS. HS-induced overexpression of sFlt1 caused severe defects in HyA formation, leading to HyA stalling toward the PLA (arrow, **H**). (**J, K**) Quantification of the number of vascular endothelial cells (vECs) that comprise the HyA, Hy loop, and hypophyseal vein (HyV) at 72 (**J**) and 144 (**K**) hpf. HS-induced overexpression of sFlt1 led to a drastic reduction in the number of vECs that comprise the HyA and milder reduction of vEC numbers in Hy loop. In contrast, sFlt4 overexpression displayed no effect on the number of vECs that comprise the Hy loop and HyV, but caused a significant reduction in HyA vEC numbers at 144 hpf (**K**). The number of animals examined per treatment at 72 hpf: without HS treatment, n=11 for control, n=11 for *sflt1*, and n=10 for *sflt4*; with HS treatment, n=20 for control, n=25 for *sflt1*, and n=20 for *sflt4*. The number of animals examined at 144 hpf: without HS treatment, n=25 for control, n=11 for *sflt1*, and n=18 for *sflt4*; with HS treatment, n=15 for control, n=22 for *sflt1*, and n=21 for *sflt4*. In panels (**D**), (**J**), and (**K**), each data point shown in magenta represents individual animal's quantification, and values represent means ± SD (*, **, ***, and **** indicate $p<0.05$, $p<0.01$, $p<0.001$, and $p<0.0001$, respectively, by one-way analysis of variance [ANOVA] followed by Tukey's HSD test). Scale bar: 50 μm in (**C**) for (**A–C**) and in (**I**) for (**F–I**).

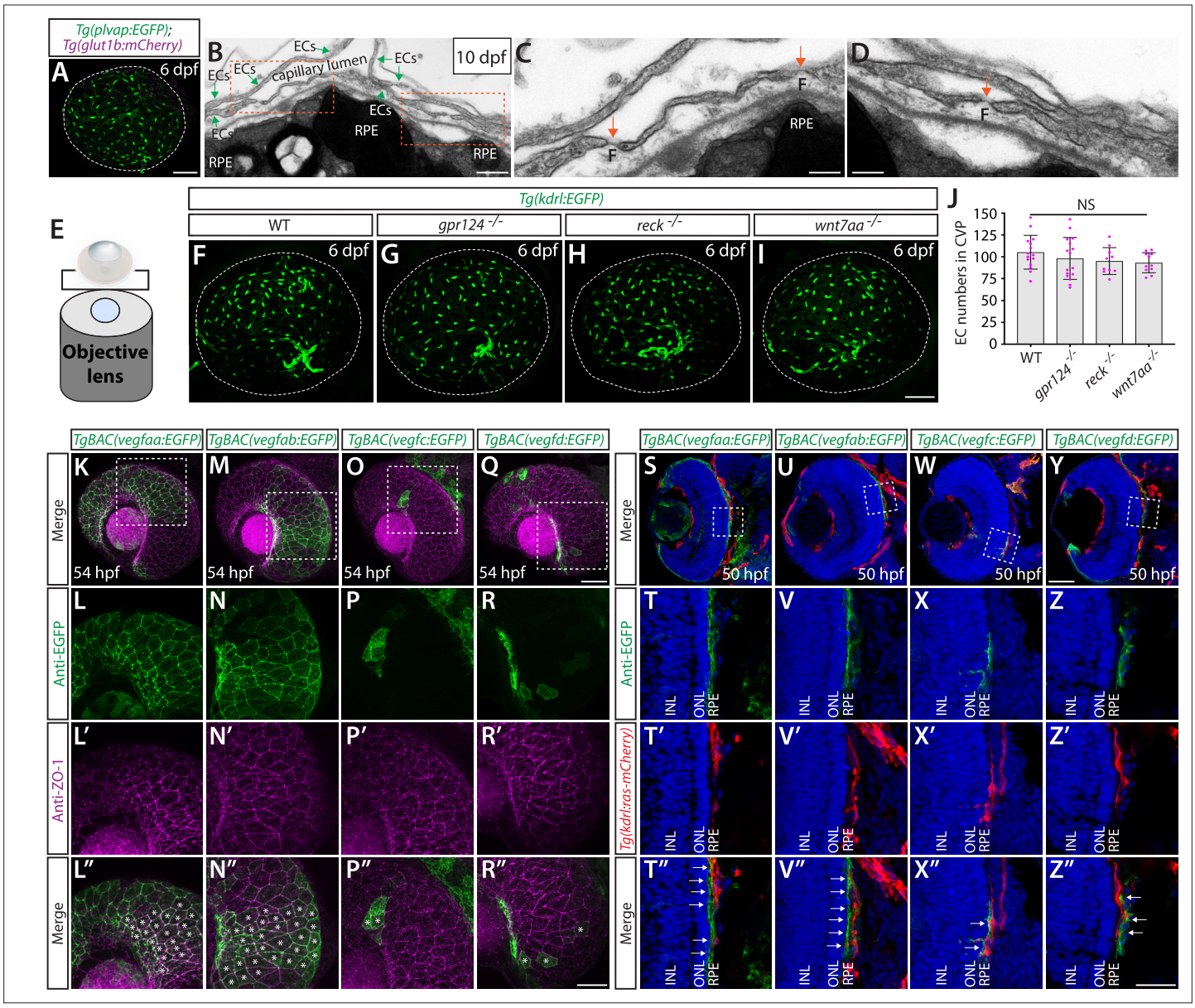

Figure 9. Normal choriocapillaris formation in zebrafish deficient for Wnt/β-catenin signaling, and conserved expression of Vegfa paralogs in retinal pigment epithelium (RPE). (**A**) Dissected eye from 10 days post fertilization (dpf) *Tg(plvap:EGFP);Tg(glut1b:mCherry)* zebrafish immunostained for GFP and DsRed shows strong *Tg(plvap*:EGFP) and absent *Tg(glut1b*:mCherry) expression in the choriocapillaris (choroidal vascular plexus, **CVP**). (**B–D**) Transmission electron microscopy images of 10 dpf wild-type (WT) outer retina focused on the CVP and RPE layer. Magnified images of the boxed areas in (**B**) show the presence of fenestrae (**F**) in the vascular endothelial cells (vECs) comprising the CVP (orange arrows, **C**, **D**). (**E**) Schematic diagram of 3D confocal CVP imaging from the back of dissected eyes. (**F–I**) WT (**F**), *gpr124*$^{-/-}$ (**G**), *reck*$^{-/-}$ (**H**), and *wnt7aa*$^{-/-}$ (**I**) CVP visualized by *Tg(kdrl*:EGFP) expression at 6 dpf. Confocal *z*-stack images of dissected eyes were taken after immunostaining for GFP. (**J**) Quantification of vECs that comprise the CVP at 6 dpf (n=15 for WT, n=16 for *gpr124*$^{-/-}$, n=10 for *reck*$^{-/-}$, and n=11 for *wnt7aa*$^{-/-}$ fish). No significant difference was observed across these genotypes. Each data point shown in magenta represents individual animal's quantification. Refer to ***Figure 9—source data 1*** for the precise cell counts of individual larvae. (**K–R″**) Lateral views of 54 hours post fertilization (hpf) *TgBAC(vegfaa:EGFP)* (**K**), *TgBAC(vegfab:EGFP)* (**M**), *TgBAC(vegfc:EGFP)* (**O**), and *TgBAC(vegfd:EGFP)* (**Q**) embryos immunostained for GFP and ZO-1, a tight junction marker for RPE. Magnified images of the boxed areas in (**K**), (**M**), (**O**), and (**Q**) are shown in (**L–L″**), (**N–N″**), (**P–P″**), and (**R–R″**), respectively. *TgBAC(vegfaa*:EGFP) and *TgBAC(vegfab*:EGFP) expression was broadly co-localized with ZO-1 immunoreactivity in RPE (asterisks in **L″**, **N″**). Sparse EGFP^{+} cells were observed in *TgBAC(vegfc:EGFP)* and *TgBAC(vegfd:EGFP)* eyes, some of which were co-localized with ZO-1 immunoreactivity (asterisks in **P″**, **R″**). (**S–Z″**) Cryosections of 50 hpf *TgBAC(vegfaa:EGFP)* (**S**), *TgBAC(vegfab:EGFP)* (**U**), *TgBAC(vegfc:EGFP)* (**W**), and *TgBAC(vegfd:EGFP)* (**Y**) embryos that carried the *Tg(kdrl:ras-mCherry)* transgene. Sections were immunostained for GFP and DsRed, and counterstained for DAPI. Magnified images of the boxed areas in (**S**), (**U**), (**W**), and (**Y**) are shown in (**T–T″**), (**V–V″**), (**X–X″**), and (**Z–Z″**), respectively. *TgBAC(vegfaa*:EGFP) and *TgBAC(vegfab*:EGFP) expression was broadly observed in the RPE layer directly adjacent to the CVP (white arrows in **T″**, **V″**). Sparse EGFP^{+} cells on *TgBAC(vegfc:EGFP)* and *TgBAC(vegfd:EGFP)* sections resided in

Figure 9 continued on next page

Figure 9 continued

close proximity to the CVP (white arrows in **X″**, **Z″**). **NL**: inner nuclear layer, **ONL**: outer nuclear layer. Scale bars: 500 nm in (**B**); 200 nm in (**C**), (**D**); 50 µm in (**A**), in (**I**) for (**F–I**), in (**Q**) for (**K**), (**M**), (**O**), in (**Y**) for (**S**), (**U**), (**W**); 30 µm in (**R″**) for (**L–L″**), (**N–N″**), (**P–P″**), (**R–R″**); 25 µm in (**Z″**) for (**T–T″**), (**V–V″**), (**X–X″**), (**Z–Z″**).

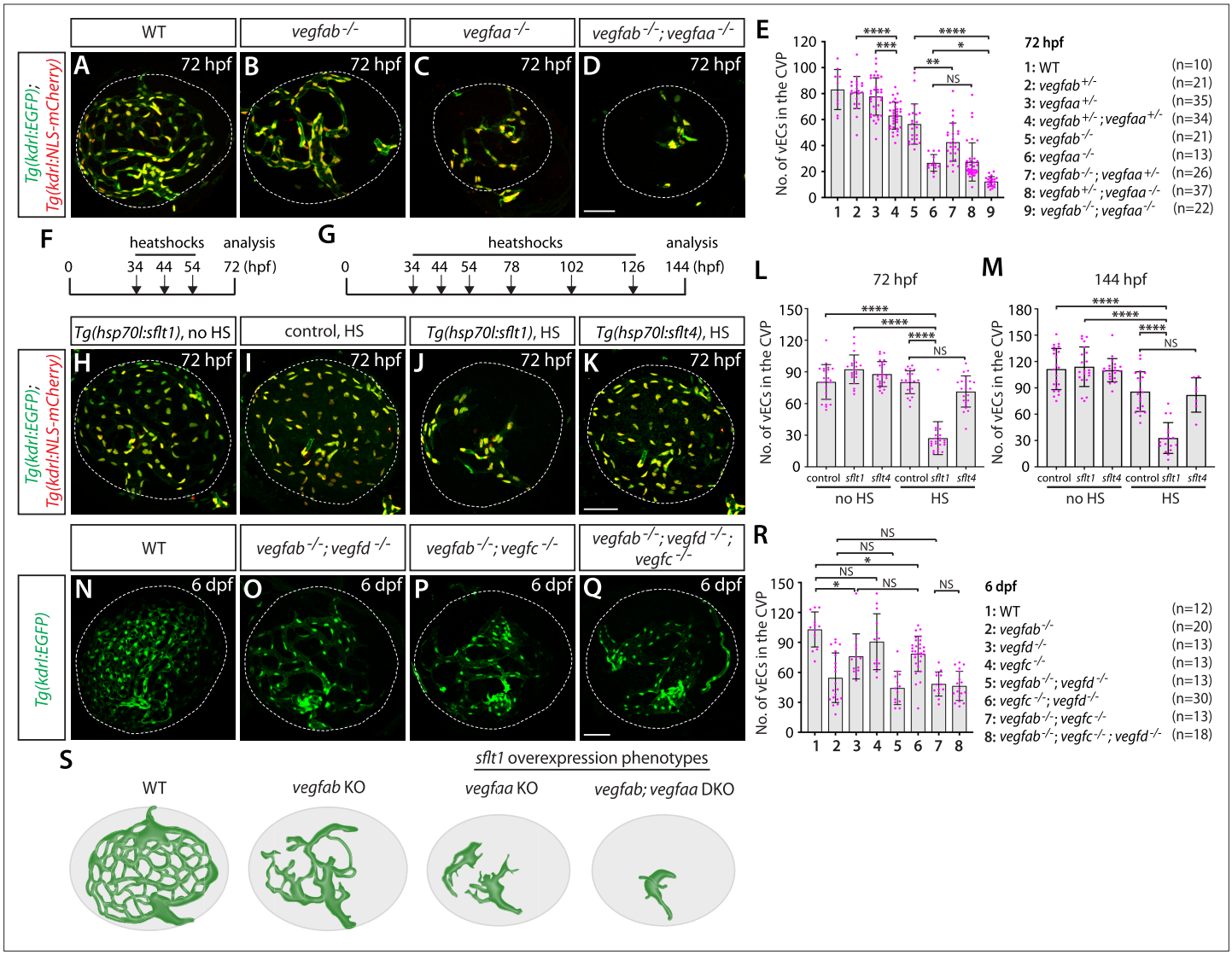

Figure 10. Zebrafish Vegfa paralogs are redundantly required for fenestrated choroidal vascular plexus (CVP) formation. (**A–D**) Wild-type (WT) (**A**), *vegfab*$^{-/-}$ (**B**), *vegfaa*$^{-/-}$ (**C**), and *vegfab*$^{-/-}$;*vegfaa*$^{-/-}$ (**D**) CVP visualized by *Tg(kdrl:*EGFP) and *Tg(kdrl:*NLS-mCherry) expression at 72 hours post fertilization (hpf). (**E**) Quantification of the number of vascular endothelial cells (vECs) that comprise the CVP at 72 hpf (the number of animals examined per genotype is listed in the panel). Zebrafish *vegfa* paralogs genetically interacted in fenestrated CVP formation. (**F, G**) Time course of the heatshock (HS) experiments for panels (**H–M**). (**H–K**) The CVP of 72 hpf *Tg(hsp70l:sflt1)* (**H, J**), *Tg(hsp70l:sflt4)* (**K**), and their control sibling (**I**) larvae that carried both the *Tg(kdrl:EGFP)* and *Tg(kdrl:NLS-mCherry)* transgenes after treatment with (**I–K**) and without (**H**) multiple HS. HS-induced overexpression of sFlt1 led to pronounced reductions in the number of vECs constituting the CVP (**J**). (**L, M**) Quantification of the number of vECs that comprise the CVP at 72 (**L**) and 144 (**M**) hpf with and without HS treatments. The number of animals examined per treatment at 72 hpf: without HS treatment, n=23 for control, n=21 for *sflt1*, and n=25 for *sflt4*; with HS treatment, n=23 for control, n=24 for *sflt1*, and n=23 for *sflt4*. The number of animals examined at 144 hpf: without HS treatment, n=22 for control, n=21 for *sflt1*, and n=20 for *sflt4*; with HS treatment, n=20 for control, n=28 for *sflt1*, and n=24 for *sflt4*. (**N–Q**) WT (**N**), *vegfab*$^{-/-}$;*vegfd*$^{-/-}$ (**O**), *vegfab*$^{-/-}$;*vegfc*$^{-/-}$ (**P**), and *vegfab*$^{-/-}$;*vegfd*$^{-/-}$;*vegfc*$^{-/-}$ (**Q**) CVP visualized by *Tg(kdrl:*EGFP) expression at 6 days post fertilization (dpf). (**R**) Quantification of the number of vECs that comprise the CVP at 6 dpf (the number of animals examined per genotype is listed in the panel). Refer to ***Figure 10—source data 1*** for the precise cell counts of individual larvae. (**S**) Schematic representations of the CVP phenotypes observed in *vegfa* mutants and after sFlt1 overexpression at 72 hpf. Temporal inhibition of Vegfa signaling by sFlt1 overexpression recapitulated the severely impaired CVP phenotypes observed in genetic mutants. In panels (**E**), (**L**), (**M**), and (**R**), each data point shown in magenta represents individual animal's quantification, and values represent means ± SD (*, **, ***, and **** indicate $p<0.05$, $p<0.01$, $p<0.001$, and $p<0.0001$, respectively, by one-way analysis of variance [ANOVA] followed by Tukey's HSD test). Scale bars: 50 µm in (**D**) for (**A–D**), in (**K**) for (**H–K**), in (**Q**) for (**N–Q**).

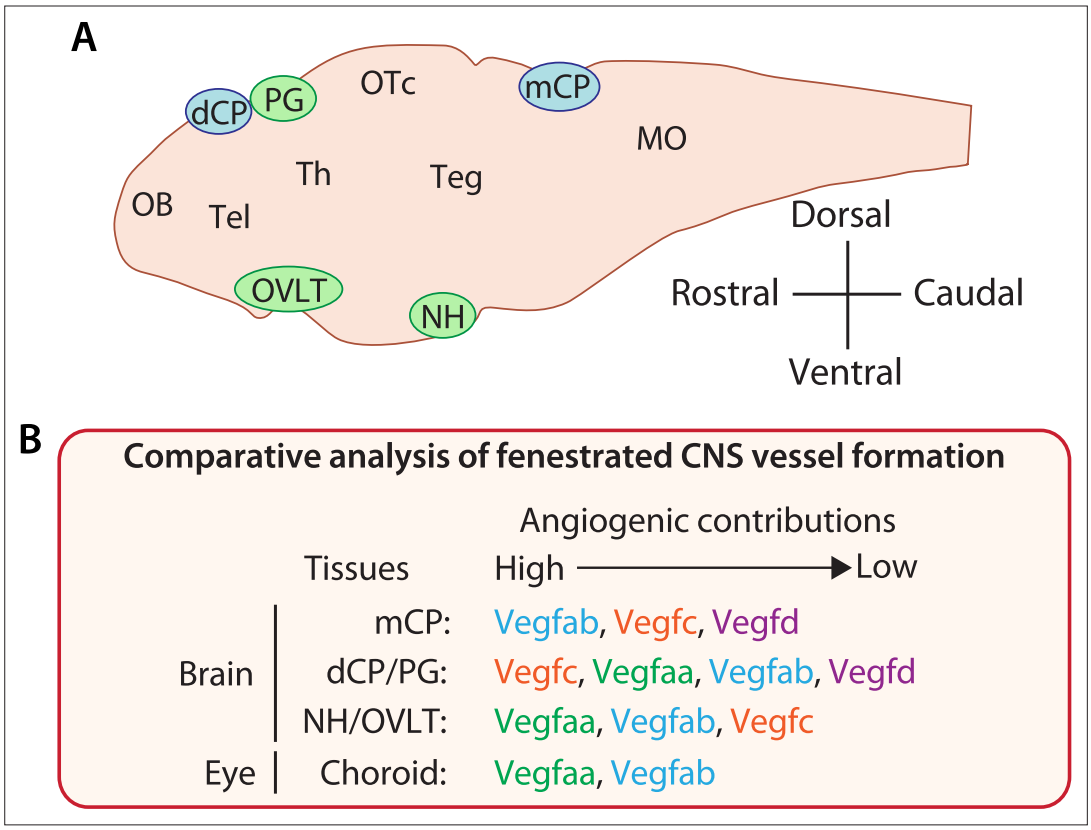

Figure 11. Comparative analysis of vascularization across fenestrated central nervous system (CNS) vascular beds reveals crucial angiogenic interplay of Vegfc/d and Vegfa in choroid plexus (CP) and circumventricular organ (CVO) vascularization. (**A**) Schematic diagram of a mid-sagittal section of the larval zebrafish brain indicates the location of the CPs and CVOs examined in our current and previous studies. MO: medulla oblongata, OB: olfactory bulb, OTc: optic tectum, Teg: tegmentum, Tel: telencephalon, Th: thalamus. (**B**) Summary of findings from our comparative analysis of fenestrated vessel formation. Angiogenic contributions were speculated based on the severity and penetrance of observed phenotypes and also on the levels of genetic interactions detected to cause phenotypes. This comparative result reveals CNS region-specific requirements for Vegfs-dependent angiogenesis and identifies an unexpected role for Vegfc/d in fenestrated brain vessel formation.